RSC Advances

ROYAL SOCIETY
OF **CHEMISTRY**

www.rsc.org/advances

Pressure Induced Structural Transformations of Anatase TiO₂ Nanotubes Probed by Raman Spectroscopy and Synchrotron X-ray Diffraction

Zhaohui Dong[1,2], Fengping Xiao[1,3], Ankang Zhao[1], Lijia Liu,[1,4, 5] T. K. Sham[1,5], and Yang Song[*, 1, 5]

[1]Department of Chemistry and [5]Soochow University-Western University Centre for Synchrotron Radiation Research, The University of Western Ontario, London, Ontario N6A 5B7, Canada

[2]Shanghai Synchrotron Radiation Facility (SSRF), Shanghai Institute of Applied Physics, CAS, Shanghai, 201204, PR China

[3]College of Chemistry and Chemical Engineering, Zhaoqing University, Zhaoqing, Guangdong, 526061, PR China.

[4]Institute of Functional Nano and Soft Materials (FUNSOM), Soochow University, Suzhou, Jiangsu, 215123, PR China

*Correspondence author. Email: yang.song@uwo.ca Phone: 519-661-2111 Ext. 86310. Fax: 519-661-3022

Abstract

Anatase titanium dioxide (TiO_2) nanotubes synthesized via electrochemical anodization were studied under high pressure up to 31 GPa. The structural transformations were characterized by *in situ* Raman spectroscopy and synchrotron X-ray diffraction. Raman measurements suggest that anatase TiO_2 nanotubes transform to amorphous phase upon compression to 17.7 GPa and remain mostly amorphous upon recovery but with minor α-PbO_2 and anatase phases as a mixture. In contrast, direct anatase to baddeleyite phase transition was unambiguously observed at ~14 GPa in the diffraction measurements. Structural refinement allows the quantitative analysis of the transition sequence and reals that the recovered phase is mostly crystalline α-PbO_2. This discrepancy can be attributed to the special surface and interfacial structure associated with the tube morphology. Moreover, the compression behavior such as the compressibility of both anatase and baddeleyite phases of TiO_2 nanotubes was examined in parallel with other nanostructured TiO_2 nanomaterials. Our analysis shows that morphology plays a more prominent role than size in affecting the high pressure behaviors of 1D TiO_2 nanomaterials compared to nanoparticles, and that the interplay of multiple factors such as morphology, size, interfacial structures, as well as lattice defects can substantially influence the phase stability and thus transformation sequence.

1. Introduction

TiO$_2$ as a wide band gap semiconductor has attracted enormous attentions due to its wide range of applications such as in photocatalysis[1], solar cell[2], optoelectronic[3], and chemical sensors[4] as well as lithium ion batteries.[5] These applications of TiO$_2$ are highly structural dependent. So far, more than six structures have been found in nature as well as in laboratory, among which anatase and rutile are the most promising structures for various practical applications. For example, anatase phase is more bioactive and robust for catalysis purposes, while rutile is often used for electronic devices due to its high dielectric constant and thermodynamic stability.[6] Therefore, understanding the structure-property relationship as well as transitions among different structures is of particular interest to develop new applications. Furthermore, nanostructured TiO$_2$ materials have demonstrate substantially enhanced performance in a number of applications compared to the corresponding bulk materials.[4,7-11] To date, nanostructured TiO$_2$ with different morphologies (e.g., nanoparticles, nanowires, nanobelts, nanotubes, nanosheets, etc.) have been successfully synthesized.[7,10-18] Compared to other nanostructured materials, 1D anatase TiO$_2$ nanomaterials, such as nanotubes and nanowires, have attracted considerable interest in particular due to their superior properties in different applications, especially in photocatalysis and solar cells.[8-11, 18]

In addition to traditional synthetic routes, pressure provides an effective tool to produce new structures and to tune the properties of materials.[19] As a result, extensive high-pressure studies have been carried out on TiO$_2$ nanomaterials especially with anatase and rutile structures over the past a few years. For instance, a number of experimental and theoretical high-pressure studies indicate that both bulk and

nanostructured TiO_2 have a series of high-pressure phases, and the sequence of phase transitions is highly size and morphology dependent. [20-43] At high pressure, both anatase and rutile bulk TiO_2 attains phases that are isostructural with columbite (orthorhombic α-PbO_2)[22] and baddeleyite[20] (monoclinic ZrO_2), following a transition sequence from anatase phase to α-PbO_2 phase and then to baddeleyite upon compression.[21-25, 27, 43, 44] However, this phase transition route is only applicable to bulk TiO_2. For TiO_2 nanomaterials, the transition sequences are different as their morphology and size vary. For instance, Wang and Saxena found that the anatase phase in TiO_2 nanoparticles (with particle size ranging from 7 to 11 nm) was stable up to 24 GPa, and then turned to an amorphous phase upon further compression.[45] The amorphous phase was found quenchable to ambient pressure. However, high-pressure study of anatase TiO_2 nanoparticles with size of 30 nm showed that a baddeleyite phase formed at 16.4 GPa without pressure-induced amorphization.[26] . Such a large discrepancy was believed due to the variation in the grain size of nanoparticles. Systematic studies on TiO_2 nanoparticles have revealed the correlation between their high-pressure behaviors and the particle size: 1) when the particle size is less than 10 nm, the nanoparticles underwent a pressure induced amorphization upon compression;[31-33, 36, 43] 2) when the size of nanoparticle is between 12 and 50 nm, the anatase phase transformed into the baddeleyite phase directly;[31, 35, 43] 3) when the particle size is larger than 50 nm, the phase transition sequence is from anatase to α-PbO_2 and then to baddeleyite phase.[23-25, 28, 31, 43]

However, such size-effects model is not applicable to 1D TiO_2 nanomaterials. In addition to the factor of size, morphology was also found to play an important role in influencing the high pressure behaviors of 1D nanomaterials. For instance, the

pressure-induced amorphization were found in TiO_2-B nanoribbons with widths in the range of 50-200 nm and thickness of ~20 nm, the size of which is far beyond the critical size of 10 nm for nanoparticles. Moreover, both our previous high-pressure study of anatase TiO_2 nanowires with size of 50-100 nm or150-200 nm and that by Li *et al.*[37] suggest a phase transition sequence from anatase to baddeleyite phase without going through the α-PbO_2 phase. Interestingly, nanostructured anatase TiO_2 in another 1D morphology, i.e., nanotubes with a tube diameter of ~8-10 nm, was found to irreversibly transform to amorphous phase with different densities upon compression and decompression, similar to nanoparticles.[40] More recently, nanostructured anatase TiO_2 with composition and morphology variations, such as Nb-doped TiO_2 nanoparticles and TiO_2 nanosheets show new interesting and unique high pressure behaviors. [29]

Despite the extensive high-pressure investigations and rationalizations of TiO_2 nanoparticles, no systematic understanding of the high-pressure behaviors of 1D TiO_2 nanomaterials, especially TiO_2 nanotubes, is available due to the extremely sparse studies.[37, 39, 40] Here we report the high-pressure study of electrochemically synthesized TiO_2 nanotubes with tube diameter of ~ 100 nm that allows the systematic study when compared with those with a significantly smaller tube diameter (i.e., ~10 nm). Interesting and new high pressure behaviors of anatase TiO_2 nanotubes that are substantially different from previous studies were observed and characterized by *in-situ* Raman spectroscopy and synchrotron X-ray diffraction. By comparison with other 1D nanostructured anatase TiO_2 particularly nanowires and nanotubes, the transformation mechanisms were examined and the morphology effect was addressed. This study contributes to the understanding of pressure tuning nanostructures involving the interplay of multiple

influencing factors including morphology, dimensions as well as interfacial structures.

2. Experimental section

2.1 Sample preparation

TiO$_2$ nanotubes were synthesized via electrochemical anodization method which offers excellent control over the length and width of the nanotubes in a certain range.[6] The experiment was carried in a customized electrochemical cell with a two-electrode configuration. The Ti foil of 0.1 mm thick (Goodfellow Ltd.) was cut into 2 cm × 1 cm pieces and rinsed with acetone and ethanol in order to remove organic impurities from the surface prior to the anodization. Ethylene glycol containing 0.25% (wt.) NH$_4$F was used as the electrolyte. The Ti foil was anodized with an applied potential of 50 V for 72 hours at room temperature. After anodization, the Ti foil was rinsed with ethanol and then dried under a N$_2$ flow. After the experiment, the surface of the Ti foil turned yellow, and the thin film of TiO$_2$ nanotubes can be easily peeled off from the substrate. The as-prepared thin film of TiO$_2$ nanotubes was then calcined at 550 °C in a furnace for two hours. After that the samples were cooled naturally to room temperature.

2.2 Characterization

Morphologies of the synthesized TiO$_2$ nanotubes were examined using scanning electron microscopy (SEM, LEO 1540 FIB/SEM)). The results showed that the TiO$_2$ nanotubes produced via electrochemical anodization under optimized conditions are closely packed with a length of 35 μm and tube diameter of ~100 nm (Fig. 1a). The as-made TiO$_2$ nanotubes were in amorphous phase as confirmed by X-ray diffraction (XRD) using Rigaku Co $K\alpha$ radiation (λ=1.7892 Å). Annealing the sample at 550 °C

successfully converted amorphous phase to anatase phase completely without influencing the tube morphology, which was also confirmed by XRD and SEM(Fig. 1a). [6]

High-pressure studies were carried out using a symmetric diamond anvil cell (DAC) with a pair of type I diamonds with a culet size of 400 μm. A hole with a diameter of 130 μm was drilled on a stainless steel gasket and used as the sample chamber. The pressure was determined by the well-established ruby fluorescence method. *In situ* Raman spectra were collected using a customized micro-Raman spectroscopy system with a diode pumped solid state laser (λ=532 nm) as the excitation source. For Raman measurements, silicon oil was used as the pressure transmitting medium (PTM). *In situ* angle-dispersive XRD measurements were carried out at room temperature at the beamline 16ID-B of HPCAT at the Advanced Photon Source. The incident wavelength of the monochromatic X-ray beam was 0.3738 Å with a beam size of 4 μm×5 μm. The diffraction data were recorded on a MAR 345 imaging plate. Neon gas was used as the PTM for XRD measurements. A motorized gear box was also employed to regulate the pressure with fine increments. The 2D Debye‒Scherrer diffraction patterns were integrated by using Fit2D program for further analysis. The structural refinement was performed using GSAS software package.

3. Results and discussion

3.1 Raman spectra of TiO$_2$ nanotubes upon compression and decompression

The anatase phase of TiO$_2$ has a space group of D_{4h}^{19} (*I*4$_1$/amd, *Z=2*). According to

factor group analysis, 15 optical modes with the following irreducible representation of normal vibrations were predicted: $1A_{1g} + 1A_{1u} + 2B_{1g} + 1B_{2u} + 3E_g + 2E_u$, among which six modes $(A_{1g}+2B_{1g}+3E_g)$ are Raman-active and three modes $(A_{1u}+2E_u)$ are infrared-active. The Raman spectra of TiO_2 nanotube collected at near ambient pressure are shown in Fig. 2 (top spectrum), where 5 prominent peaks were observed. These 5 peaks can be assigned as $E_{g(1)}$ (140 cm^{-1}), $E_{g(2)}$ (192 cm^{-1}), $B_{1g(1)}$ (390 cm^{-1}), $A_{1g}+ B_{1g(2)}$ (509 cm^{-1}) and $E_{g(3)}$ (631 cm^{-1}), respectively. The numbers labeled in the parentheses of the subscripts were used for distinguishing peaks with the same symmetry. The Raman profile is consistent with the earlier studies of both bulk materials and nanowires indicating that the synthesized TiO_2 nanotubes have a pure anatase structure.[23, 39] Compared to the bulk TiO_2, Raman modes observed in TiO_2 nanotubes show only slightly deviation in the Raman shift, which is likely due to the slight stoichiometry deviations of different morphologies from different synthetic methods, known to influence both Raman peak positions and widths.[46]

The Raman spectra of TiO_2 nanotube collected upon compression up to 17.7 GPa are shown in Fig. 2. Upon compression, all the Raman modes shifted to higher frequencies except for the $E_{g(2)}$ mode, which exhibited a red shift until its disappearance at about 3 GPa. Upon compression, the intensity of all the peaks associated with the anatase phase gradually became weak. At 17.7 GPa, all the Raman modes were significantly suppressed leaving only one peak discernable at ~ 183 cm^{-1}, indicating that the sample was highly disordered at high pressure. Other than the profile broadening, no distinguishable new peak was observed, suggesting no phase transition below 17.7 GPa.

The reversibility of pressure effect on crystal structures provides important information on transformation mechanisms. Therefore, after sample was compressed to 17.7 GPa, Raman measurements of TiO_2 nanotubes were also conducted upon decompression. In general, the intensity of all the Raman peaks increased gradually as pressure decreasing, and all the Raman modes shifted to lower frequencies. At 4.6 GPa, a new peak appeared at 161 cm^{-1} indicating a possible phase transition. This new peak shifts to 148 cm^{-1} at 0.1 GPa. According to the reference values, this peak can be associated with the $\alpha\text{-}PbO_2$ phase.[39] The rest four peaks can be assigned to the recovered anatase phase although all the Raman peaks shift to slightly higher frequencies than before compression. Thus the retrieved phase can be interpreted as the mixture of the anatase phase and $\alpha\text{-}PbO_2$ phase. The large variation in the Raman profile can be attributed to the pressure induced structural modification, which is mostly irreversible upon compression.

3.2 X-ray diffraction patterns of TiO_2 nanotubes upon compression and decompression

In situ high-pressure XRD measurements on TiO_2 nanotubes upon compression up to ~31 GPa followed by decompression are depicted in Fig. 3. As can be seen, all the reflections at near ambient pressure (i.e., ~ 0.9 GPa) can be indexed to the pure anatase phase with cell parameters of $a = b = 3.8068$ Å, $c = 9.5233$ Å, and $V = 138.01$ Å^3, consistent with the bulk anatase TiO_2 materials (JCPDS file 84-1286). Upon compression, all the reflections of anatase TiO_2 shift to higher 2θ angle, suggesting a pressure-induced reduction of d-spacings or shrinkage of the unit cell. When the pressure

was increased to 14.7 GPa, two reflections appeared at 7.3198º and 8.0128º, which are associated with the reflections of (1 1 -1) and (1 1 1), respectively for baddeleyite phase as clearly shown in the structural refinement in Fig. 4a, indicating the onset phase transformation from anatase to baddeleyite phase. Above 14.7 GPa, reflections corresponding to anatase were suppressed significantly. All the reflections of anatase phase disappeared at 19.0 GPa, which suggests the completion of the anatase phase to baddeleyite phase transformation as strongly supported by the structural refinement profile (Fig. 4b). At the highest pressures of 31.1 GPa, the sample is in pure baddeleyite phase as all the reflections were indexed with the baddeleyite structure. At this pressure, all the reflections were broadened significantly, but still clearly distinguishable, suggesting the samples were somehow disordered but still in a crystalline phase.

Upon decompression, all the reflections shift to lower 2θ angle gradually, indicating the expansion of the unit cells. As shown in Fig. 3, when the pressure was decreased to 4.9 GPa, a new reflection appeared at 7.5595º, suggesting the onset of a phase transition. The new phase persisted down to ambient pressure, at which all reflections of the baddeleyite phase disappeared completely. The XRD pattern can be interpreted by the single α-PbO_2 phase by structural refinement (Fig. 4c), suggesting that the sample is in almost pure α-PbO_2 phase.

3.3 Discussion

Apparently, Raman measurements and X-ray diffraction patterns suggested strongly contrasting high-pressure behaviors of the same TiO_2 nanomaterials. First of all, it is well known that upon compression, anatase bulk TiO_2 undergoes a phase transition sequence

from anatase phase to α-PbO$_2$ phase, and then to baddeleyite phase.[22, 23] For nanostructured TiO$_2$ materials such as nanoparticles and nanowires, however, anatase phase generally transforms directly into baddeleyite phase upon compression.[31, 34, 37, 39, 43] Table I summarizes the phase transition sequences of different TiO$_2$ materials. For TiO$_2$ nanoparticles in particular, the phase transition sequences are found strongly particle size dependent. The anatase to baddeleyite phase transitions was found only in the mid-sized TiO$_2$ nanoparitcles (i.e., 12-50 nm). Outside this range, the TiO$_2$ nanoparticles exhibit either same phase transition sequence as bulk materials (when > 50 nm) or become amorphous (when < 12 nm) upon compression. Our previous studies on anatase TiO$_2$ nanowires with different wire diameters suggest that the transition sequence is not size dependent and follows that of mid-sized nanoparticles. In this study, given the electrochemically synthesized TiO$_2$ nanotubes are several tens of microns long (i.e., comparable to bulk materials), the tube diameter thus is the determining dimension. Even though the tube diameter of 100 nm is two times larger than the critical size of 50 nm for nanoparticles, the deletion of the α-PbO$_2$ phase is still found upon compression. This observation is similar to that of anatase TiO$_2$ nanowires with similar or larger sizes.[37, 39] Therefore, it is reasonable to conclude that, in contrast to nanoparticles, morphology has more prominent effect than size in affecting high pressure behaviors of 1D TiO$_2$ nanomaterials. So far, there were several attempts to explain why α-PbO$_2$ phase was hindered in anatase TiO$_2$ nanomaterials. A widely accepted interpretation was that nanostructured TiO$_2$ has enhanced surface energy compared to the bulk counterparts, although some other factors such as imperfections of the crystals may also contribute.[30,

[35, 43] Nonetheless, the rational correlation between the phase stability and dimensions of the nanostructures is still not fully understood.

In the Raman measurements, contrastingly, no phase transition is found upon compression up to 17.7 GPa, a pressure substantially higher than the transition onset pressure (i.e., ~ 14 GPa) found in the XRD measurements. In the case of TiO_2 nanowires, Raman measurements clearly suggests the anatase-to- baddeleyite transition at similar pressures, consistent with the XRD measurements.[39] We then closely examined the difference between these different experiments. We noted that silicon oil was used as the PTM in Raman measurements while neon was used in the XRD experiments. Although neon provides a better hydrostatic condition above 10 GPa than silicon oil, the difference in the hydrostaticity is unlikely the primary factor for the different compression behavior of TiO_2 nanotubes. Given the large tube diameter and open end morphology, as well as the chemical inertness, the interaction between PTM with different molecular sizes and TiO_2 nanotubes is expected to be similar. Indeed, in Li *et al.*'s similar study on TiO_2 nanotubes where 4:1 methanol-ethanol mixture as PTM was used, it was believed that PTM can penetrate into the tubes even with much a smaller diameter (i.e., ~ 5 nm).[40] Based on these analyses, we believe TiO_2 nanotubes in the current study have substantially different and more complicated surface or interfacial structures than nanowires studied before or the nanotubes in Li's study. In particular, the large tube diameter (i.e., ~ 100 nm) and the thickness (i.e., ~ 10 nm) as well as the way the tubes are aligned upon production may result in a much more inhomogeneous pressure response along the axial direction upon compression. As a result, the inner part of the tube and tube surface layers may undergo different transition sequence. Considering that Raman

spectroscopy is a surface sensitive probe while that bulk penetrating X-ray provides information involving long-range orderness, we may conclude that the bulk TiO_2 nanotubes and especially the inner layers transform to baddeleyite phase whereas the surface layers become amorphous upon compression.

In order to further reconcile the "discrepancy" between Raman and XRD measurements as well as to probe the transition mechanism, the full width at half maximum (FWHM) of the most intense $E_{g(1)}$ mode for TiO_2NT is plotted in Fig. 5. Two tuning points (labeled as P_1 and P_2) are found at 6 GPa and 14 GPa, respectively, consistent with the observation in TiO_2 nanowires reported before.[39] For TiO_2 nanowires, P_2 coincides with the anatase to baddeleyite phase transition pressure. Interestingly, the P_2 in the current study, which is 14 GPa, is as also coincidental with the anatase to baddeleyite phase transition pressure identified in the XRD measurements. This coincidence may suggest that the anatase to baddeleyite phase did occur, although undetectable in the Raman measurements given the above discussion. Based on our earlier high-pressure study of TiO_2 nanowires, these two turning points are consistent with the three-stage process proposed for the phase transition, which involves the competition between formations of the α-PbO_2 phase and baddeleyite phase. In the first stage (0 GPa $-$ P_1), specifically, the anatase to α-PbO_2 phase transition route may be favored. However, due to the enhanced surface energy, a high energy barrier for the formation of the α-PbO_2 structure could substantially delay the transition to the α-PbO_2 phase.[45] Therefore, before the α-PbO_2 phase is eventually formed, the baddeleyite phase became the more energetically favored structure in competition with the α-PbO_2 phase at the second stage (P_1 $-$ P_2), as seen in Fig. 5. At the third stage ($>P_2$), the phase

transformation followed anatase-to-baddeleyite route monotonically, accompanied by the significantly faster increase in the FWHM of the $E_{g(1)}$ mode than the first two stages.

Furthermore, detailed analysis of XRD results of TiO_2 nanotubes allows the understanding of the pressure dependence of unit cell parameters as well as the compressibility in comparison with earlier studies of bulk and nanostructured TiO_2 materials. The normalized unit cell lengths (i.e., a/a_0 and c/c_0) as a function of pressure for the TiO_2 nanotubes are plotted in Fig. 6 in comparison with the corresponding bulk materials. First of all, c-axis exhibits a linear compressibility that is three times larger than a-axis, consistent with earlies studies on bulk TiO_2 [24, 47] as well as TiO_2 nanowires.[37, 39] The different compressibilities are believed to be associated with the intrinsic anatase crystal structure. Specifically, there are four occupied TiO_6 octahedra and four empty O_6 octahedra per unit cell. The Ti atom inside the occupied octahedra (TiO_6) makes the polyhedra much harder to compress than the empty ones (O_6). Thus the higher compressibility of the c-axis than the a-axis can be interpreted in terms of the difference in the directional population of the hard occupied (TiO_6) and soft empty (O_6) oxygen octahedra. The specific c/a compression ratio further indicates a consequence of the alignment of the empty O_6 octahedra along the c-axis and of the greater density of atoms along the a- and b-axes than along the c-axis. Moreover, compared to bulk TiO_2, the c-axis of TiO_2 nanotubes shows higher compressibility, while the compressibility along a-axis is similar. In general, the c-axis for all the nanostructured anatase TiO_2 is more compressible than the corresponding bulk material, indicating that the morphology and the crystalline growth direction of TiO_2 nanomaterials play an important role in the anisotropic behavior.[34, 37]

The pressure-volume data of TiO_2 nanotubes are shown in the Fig. 7. By fitting the third-order Birch-Murnaghan equation of state, the bulk modulus (B_0) of the anatase and baddeleyite phases for TiO_2 nanotubes obtained are 164.2 GPa and 182.8 GPa, respectively, with the first derivative (B_0') fixed at 4. For comparison purposes, the bulk modulus of the anatase phase of corresponding bulk materials, nanoparticles and nanowires are plotted together with TiO_2 nanotubes. Similar to Li *et al.*'s study on TiO_2 nanotubes with a much smaller diameter (i.e., ~ 10 nm) for which the bulk modulus was reported to be 158 GPa, the bulk modulus of TiO_2 nanotubes in current study (i.e., 164 GPa) is also slightly lower than that of TiO_2 bulk materials (i.e., 179 GPa), indicating the dimension of the TiO_2 nanotubes has a negligible influence in the compressibility. In contrast, other nanostructured TiO_2 materials such as nanowires and nanoparticles showed substantially enhanced bulk modulus, e.g., 226.5 GPa and 243 GPa, respectively. In addition, morphology-induced alterations of bulk modulus have been reported in high-pressure studies of other TiO_2 nanomaterials. For example, strongly contrasting compressibilities were observed for TiO_2 nanoparticles with rod and rice shapes.[34] The bulk modulus of rod-shaped particles was reduced, whereas that of the rice-shaped particles was enhanced by over 50% relative to the corresponding bulk materials.[34] All these observations suggest that morphology plays a dominant role in the compressibility of different TiO_2 nanostructures due to the different contribution of surface energy states.

Another interesting observation is that the baddeleyite phase exhibited a much higher bulk modulus in TiO_2 nanotubes than nanowires (182.8 GPa vs 127.8 GPa).[39] The SEM image of the recovered materials (Fig. 1b) shows that although the alignment of the nanotubes was substantially modified, the tube morphology is still clearly

distinguishable. The preservation of the morphology on compressed materials has great implications for new applications and has been reported for TiO_2 nanowires and nanotubes before.[37, 40] In addition to the open-end tube morphology and use of PTM as important factors, we believe the high stillness of baddeleyite lattice during the anatase-to-baddeleyite transition in TiO_2 nanotube also contributes to the to the morphology stability upon compression. Indeed, in our earlier studies of TiO_2 nanowires for which the baddeleyite phase has a lower stiffness, the wire morphologies were not preserved.[39]

Finally, the interplay of multiple factors must be considered collectively to interpret the different mechanical properties, phase stability as well as transition sequence of nanomaterials. Park *et al.* suggested that bulk modulus may be influenced by the crystal growth directions of TiO_2 nanomaterials.[34] For instance, the anatase TiO_2 nanorods grown along the *a*-axis showed a lower bulk modulus (243 GPa) than TiO_2 nanorices grown along the *c*-axis (319 GPa). Li *et al.* obtained the similar results in the study of anatase TiO_2 nanowires.[37] Their nanowires have the same growth direction as the nanorods, given a similar bulk modulus of 176 GPa as the bulk counterpart (179 GPa). Therefore, we can infer that the primary growth direction of TiO_2 synthesized in this study is also along *a*-axis. However, our TiO_2 nanotubes exhibit a "normal" transition sequence whereas those produced by Li *et al.* suggest that only amorphous TiO_2 with different densities was observed upon compression.[40] Crystalline defects and lattice impurities, which strongly depend on synthetic methods, can substantially influence the structural stabilities at the nanoscale.[48, 49] Indeed, plenty of crystal defects were identified in hydrothermally synthesized TiO_2 nanomaterials.[40] Our Raman results on electrochemically synthesized

TiO$_2$ nanotubes suggest inhomogeneous interfacial structures, from which crystal defects can also be inferred, but likely with a different distribution along and across the nanotubes at nanoscale. Ultimately, it would be of great interest to fabricate energy devices based on TiO$_2$ nanotubes produced via different routes both in the as-made form and retrieved from compression and to test the performance comparatively for practical applications.

4. Conclusions

In summary, anatase TiO$_2$ nanotubes synthesized by electrochemical anodization method were investigated under high pressure using *in situ* Raman spectroscopy and synchrotron X-ray diffraction. No phase transition other than amorphization was observed up to 17.7 GPa in the Raman measurements upon compression. In strong contrast, the anatase to baddeleyite phase transition was identified at 14 GPa in the XRD measurements. After pressure was released, a mixture of anatase and α-PbO$_2$ phases was retrieved indicated by the Raman measurements, whereas pure α-PbO$_2$ phase was identified in the structural refinement of XRD pattern. This discrepancy was interpreted by a special interfacial structural model leading to inhomogeneous compression behavior and corroborated with a three-stage transition process supported by monitoring the profile evolution of the most intense E_g Raman mode. Moreover, compressibility of unit cell along different axes and overall volume compressibility were studied and understood in parallel with other TiO$_2$ nanomaterials especially 1D nanostructures. Our detailed analysis suggests that morphology plays a more important role than size in affecting high pressure behaviors of 1D TiO$_2$ nanomaterials. More importantly, multiple factors including morphology, size, interfacial structures, as well as lattice defects must be

considered collectively to interpret the different compression sequences and compressibilities of different TiO_2 nanomaterials.

Acknowledgements

Notes and references

1. J. Augustynski, *Electrochim. Acta*, 1993, **38**, 43-46.
2. M. Mattesini, J. S. de Almeida, L. Dubrovinsky, N. Dubrovinskaia, B. Johansson and R. Ahuja, *Phys. Rev. B*, 2004, **70**, 115101.
3. E. J. W. Crossland, N. Noel, V. Sivaram, T. Leijtens, J. A. Alexander-Webber and H. J. Snaith, *Nature*, 2013, **495**, 215-219.
4. M. I. Baraton and L. Merhari, *J. Eur. Ceram. Soc.*, 2004, **24**, 1399-1404.
5. M. Zukalová, M. Kalbáč, L. Kavan, I. Exnar and M. Graetzel, *Chem. Mater.*, 2005, **17**, 1248-1255.
6. L. Liu, J. Chan and T.-K. Sham, *J. Phys. Chem. C*, 2010, **114**, 21353-21359.

7. T. Kasuga, M. Hiramatsu, A. Hoson, T. Sekino and K. Niihara, *Langmuir*, 1998, **14**, 3160-3163.
8. B. Liu, K. Nakata, S. Liu, M. Sakai, T. Ochiai, T. Murakami, K. Takagi and A. Fujishima, *J. Phys. Chem. C*, 2012, **116**, 7471-7479.
9. H. Tokudome and M. Miyauchi, *Chem. Commun.*, 2004,**8**, 958-959.
10. J. M. Wu, H. C. Shih and W. T. Wu, *Nanotechnology*, 2006, **17**, 105-109.
11. A. Rendón-Rivera, J. A. Toledo-Antonio, M. A. Cortés-Jácome and C. Angeles-Chávez, *Catal. Today*, 2011, **166**, 18-24.
12. Z. Miao, D. S. Xu, J. H. Ouyang, G. L. Guo, X. S. Zhao and Y. Q. Tang, *Nano Lett.*, 2002, **2**, 717-720.
13. P. Hoyer, *Langmuir*, 1996, **12**, 1411-1413.
14. S. T. Aruna, S. Tirosh and A. Zaban, *J. Mater. Chem.*, 2000, **10**, 2388-2391.
15. H. M. Cheng, J. M. Ma, Z. G. Zhao and L. M. Qi, *Chem. Mater.*, 1995, **7**, 663-671.
16. B. D. Yao, Y. F. Chan, X. Y. Zhang, W. F. Zhang, Z. Y. Yang and N. Wang, *Appl. Phys. Lett.*, 2003, **82**, 281-283.
17. Q. J. Li, R. Liu, B. Zou, T. Cui and B. B. Liu, *Physica B*, 2014, **445**, 42-47.
18. H. Y. Zhu, X. P. Gao, Y. Lan, D. Y. Song, Y. X. Xi and J. C. Zhao, *J. Am. Chem. Soc.*, 2004, **126**, 8380-8381.
19. A. San-Miguel, *Chem. Soc. Rev.*, 2006, **35**, 876-889.
20. H. Sato, S. Endo, M. Sugiyama, T. Kikegawa, O. Shimomura and K. Kusaba, *Science*, 1991, **251**, 786-788.
21. L. G. Liu and T. P. Mernagh, *Eur. J. Mineral.*, 1992, **4**, 45-52.
22. J. Haines and J. M. Leger, *Physica B*, 1993, **192**, 233-237.
23. K. Lagarec and S. Desgreniers, *Solid State Commun.*, 1995, **94**, 519-524.
24. T. Arlt, M. Bermejo, M. A. Blanco, L. Gerward, J. Z. Jiang, J. S. Olsen and J. M. Recio, *Phys. Rev. B*, 2000, **61**, 14414-14419.
25. T. Sekiya, S. Ohta, S. Kamei, M. Hanakawa and S. Kurita, *J. Phys. Chem. Solids*, 2001, **62**, 717-721.
26. Z. W. Wang, S. K. Saxena, V. Pischedda, H. P. Liermann and C. S. Zha, *J. Phys. - Condens. Matter*, 2001, **13**, 8317-8323.
27. S. Kurita, S. Ohta and T. Sekiya, *High Pressure Res.*, 2002, **22**, 319-323.
28. T. Sekiya, M. Okumura, S. Kurita and N. Hamaya, *High Pressure Res.*, 2003, **23**, 333-338.
29. Q. Li, B. Cheng, B. Tian, R. Liu, B. Liu, F. Wang, Z. Chen, B. Zou, T. Cui and B. Liu, *RSC Adv.*, 2014, **4**, 12873-12877.
30. V. Swamy, L. S. Dubrovinsky, N. A. Dubrovinskaia, F. Langenhorst, A. S. Simionovici, M. Drakopoulos, V. Dmitriev and H. P. Weber, *Solid State Commun.*, 2005, **134**, 541-546.
31. V. Swamy, A. Kuznetsov, L. S. Dubrovinsky, R. A. Caruso, D. G. Shchukin and B. C. Muddle, *Phys. Rev. B*, 2005, **71**,184302.
32. V. Pischedda, G. R. Hearne, A. M. Dawe and J. E. Lowther, *Phys. Rev. Lett.*, 2006, **96**,035509.
33. V. Swamy, A. Kuznetsov, L. S. Dubrovinsky, P. F. McMillan, V. B. Prakapenka, G. Shen and B. C. Muddle, *Phys. Rev. Lett.*, 2006, **96**,135702.
34. S.-w. Park, J.-t. Jang, J. Cheon, H.-H. Lee, D. R. Lee and Y. Lee, *J. Phys. Chem. C*, 2008, **112**, 9627-9631.

35. Y. J. Wang, Y. S. Zhao, J. Z. Zhang, H. W. Xu, L. P. Wang, S. N. Luo and L. L. Daemen, *J. Phys. : Condens. Matter*, 2008, **20**, 125224.
36. V. Swamy, A. Y. Kuznetsov, L. S. Dubrovinsky, A. Kurnosov and V. B. Prakapenka, *Phys. Rev. Lett.*, 2009, **103**,075505.
37. Q. Li, B. Cheng, X. Yang, R. Liu, B. Liu, J. Liu, Z. Chen, B. Zou, T. Cui and B. Liu, *J. Phys. Chem. C*, 2013, **117**, 8516-8521.
38. V. Swamy, *Phys. Chem. Chem. Phys.*, 2014, **16**, 18156-18162.
39. Z. H. Dong and Y. Song, *Can. J. Chem.*, 2015, **93**, 165-172.
40. Q. Li, R. Liu, T. Wang, K. Xu, Q. Dong, B. Liu, J. Liu and B. Liu, *AIP Adv.*, 2015, **5**, 097128.
41. Y. W. Huang, W. T. Li, X. T. Ren, Z. H. Yu, S. Samanta, S. Yan, J. Zhang and L. Wang, *Radiat. Phys. Chem.*, 2016, **120**, 1-6.
42. V. Swamy, L. S. Dubrovinsky, N. A. Dubrovinskaia, A. S. Simionovici, M. Drakopoulos, V. Dmitriev and H.-P. Weber, *Solid State Commun.*, 2003, **125**, 111-115.
43. G. R. Hearne, J. Zhao, A. M. Dawe, V. Pischedda, M. Maaza, M. K. Nieuwoudt, P. Kibasomba, O. Nemraoui, J. D. Comins and M. J. Witcomb, *Phys. Rev. B*, 2004, **70**,134102.
44. T. Ohsaka, S. Yamaoka and O. Shimomura, *Solid State Commun.*, 1979, **30**, 345-347.
45. Z. W. Wang and S. K. Saxena, *Solid State Commun.*, 2001, **118**, 75-78.
46. J. C. Parker and R. W. Siegel, *Appl. Phys. Lett.*, 1990, **57**, 943-945.
47. M. Calatayud, P. Mori-Sanchez, A. Beltran, A. M. Pendas, E. Francisco, J. Andres and J. M. Recio, *Phys. Rev. B*, 2001, **64**, 184113.
48. R. Schaub, E. Wahlstrom, A. Ronnau, E. Laegsgaard, I. Stensgaard and F. Besenbacher, *Science*, 2003, **299**, 377-379.
49. J. Li, Z. Q. Wang, A. K. Zhao, J. Wang, Y. Song and T. K. Sham, *J. Phys. Chem. C*, 2015, **119**, 17848-17856.

Table 1 Summary of high pressure studies of anatase TiO_2 in different morphologies and sizes

Starting TiO₂		Phase transition pressure (GPa)[b]	Bulk modulus (GPa)		Experimental method
Morphology	Size[a] (nm)		Anatase	Baddeleyite	
Bulk		4.3 – 4.6			Raman[28]
		~ 5 (12 – 15)			Raman[43]
		5.4 (~ 10)	59		XRD[22]
		4.5 – 7 (13 – 17)			Raman[23]
		4.5 (~ 13)	179	290	XRD[24]
Nano -particles	4	> 24			Raman[31]
	8	> 21			Raman[31]
	7 – 11	> 24			Raman[26]
	12	~ 18			Raman[43]
	20	15 – 16			Raman[31]
	32	11 – 15			Raman & XRD[31]
	30 – 34	18 – 20	243		XRD[42]
Nanosheets	l:20-40 t:5-8	14.6-22.8	317		Raman & XRD[29]
Nanowires	50 – 100	~ 14	266.5	127.8	Raman & XRD[39]
	150 – 250	~ 9	188.3	114.8	Raman & XRD[39]
	50 – 200	~9	176		Raman & XRD[37]
Nanotubes	8 – 10	~17.9	166		XRD[40]
	~100	~14	164.2	203.3	Raman & XRD [c]

a. The column shows particle size, length, tube diameters for nanoparticles, nanowires and nanotubes, respectively.   For nanosheets, l and t are side length and the sheet thickness.

b. The column shows phase transition pressures in TiO_2. For the bulk row, values outside and inside the parentheses are the phase transition pressures for the anatase to α-PbO_2 phase transition and α-PbO_2 to baddeleyite phase transition, respectively. For the nanoparticles row, the italic values indicate transition pressures for the anatase to amorphous phase transition. The rest values are transition pressures for the direct anatase to baddeleyite phase transition.

c. This work.
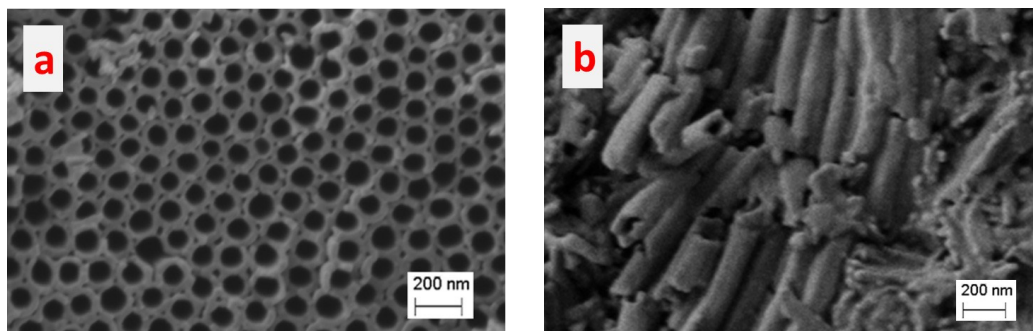
Fig. 1. SEM images of TiO$_2$ nanotubes collected before (a) and after (b) the compression and decompression cycle.
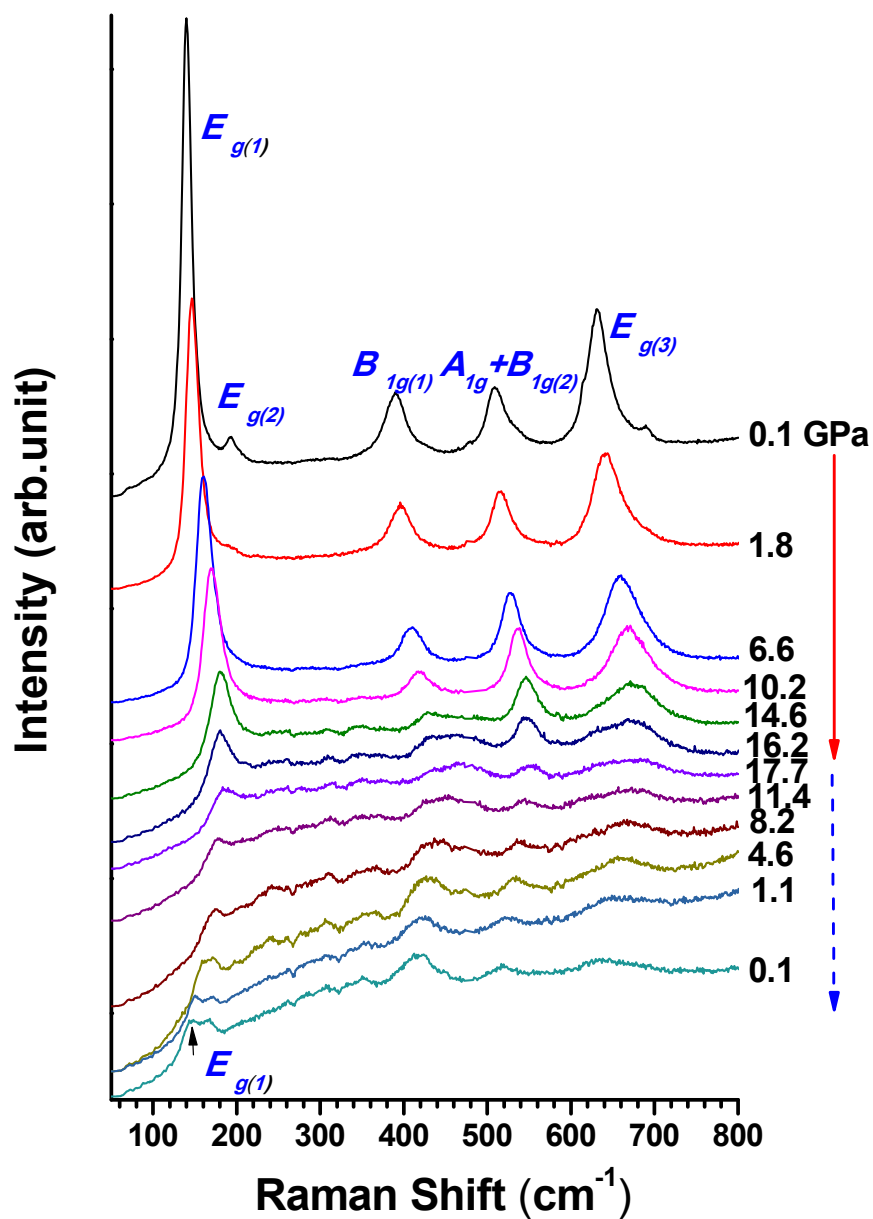
Fig. 2. Selected Raman spectra of TiO_2 nanotubes upon compression and decompression. Pressure in GPa for each spectrum is labeled. The solid and dashed lines indicate the compression and decompression sequence, respectively. All the spectra are offset for clarity. The arrow indicates the $E_{g(1)}$ Raman mode retrieved after compression.
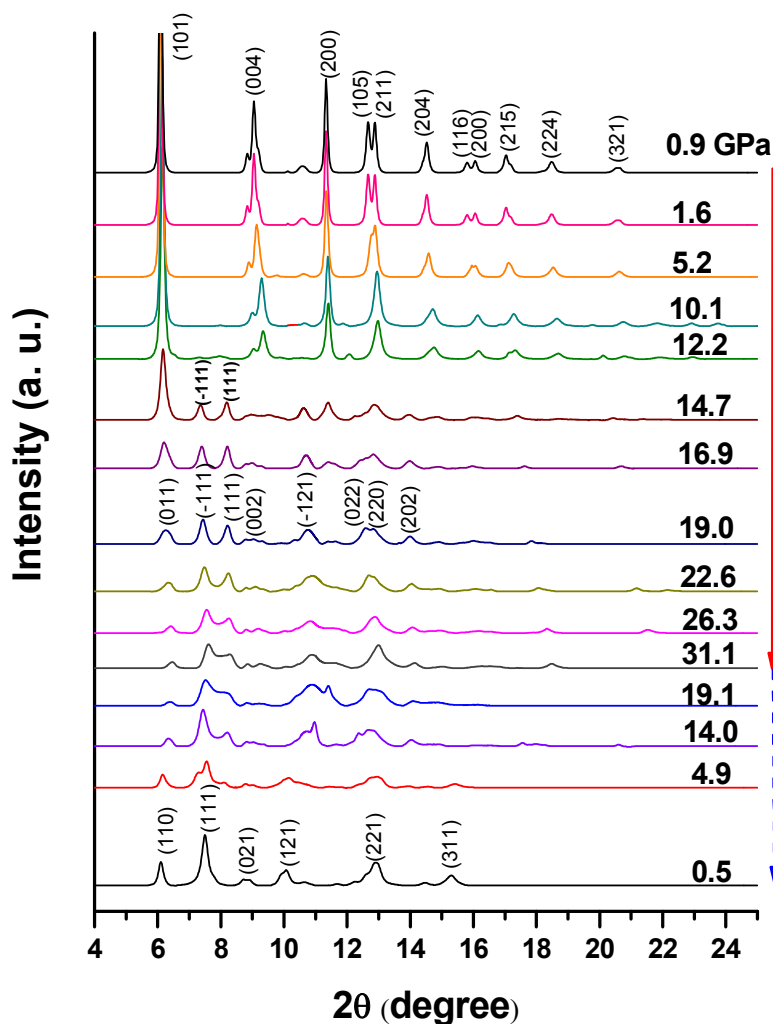
Fig. 3. Angle-dispersive background corrected X-ray diffraction patterns for TiO_2 nanotubes upon compression and decompression using synchrotron radiation (λ=0.3738 Å). The experimental pressure in GPa was labeled beside each pattern. The solid and dashed arrows indicate the compression and decompression sequences, respectively. Typical reflections of anatase phase, baddeleyite phase, and α-PbO_2 phase were indexed and labeled above the corresponding patterns at 0.9 GPa, 19 GPa upon compression, and 0.5 GPa upon decompression, respectively.
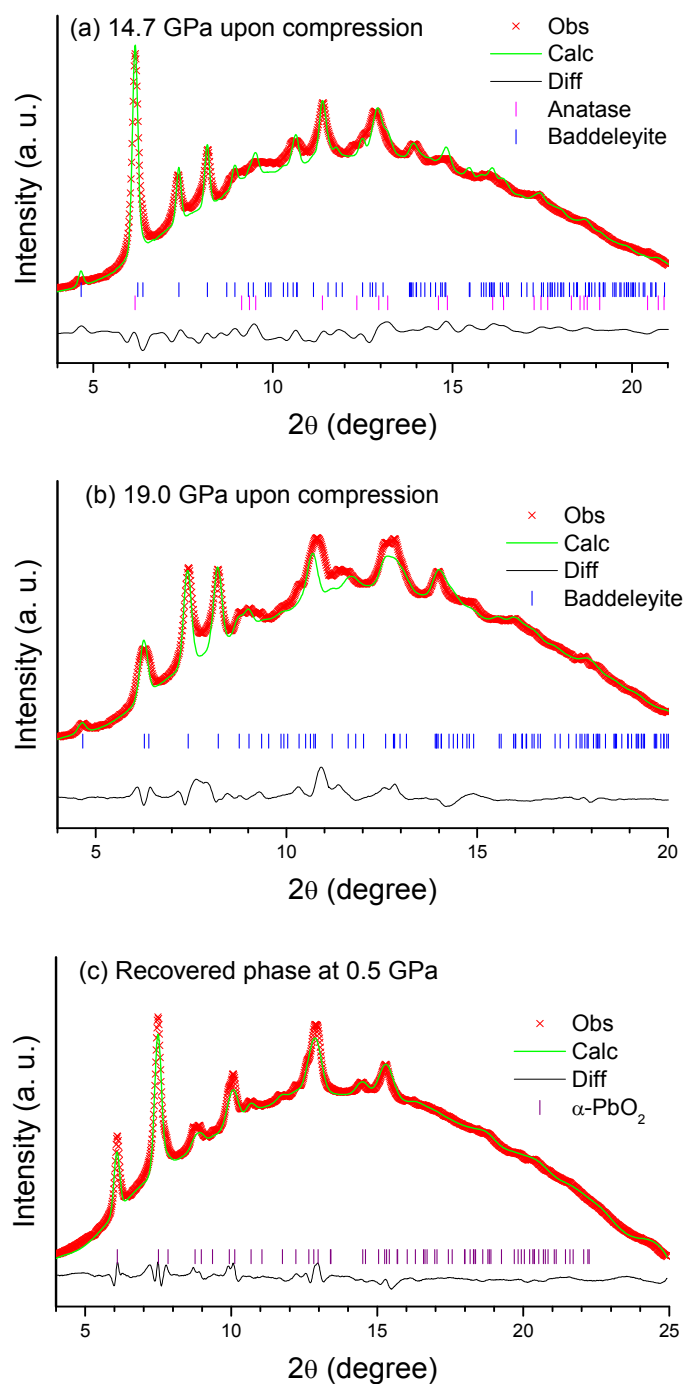
Fig. 4. Rietveld refinement of XRD patterns at 14.7 GPa (a) and 19 GPa upon compression (b) and the recovered phase at 0.5 GPa (c). The red crosses denote the experimental X-ray intensity, whereas the green solid line represents the calculated diffraction pattern based on refinement. The black curve at the bottom shows the difference between the calculated and experimental intensities. The vertical bars indicate the characteristic reflections associate with the crystal structure.
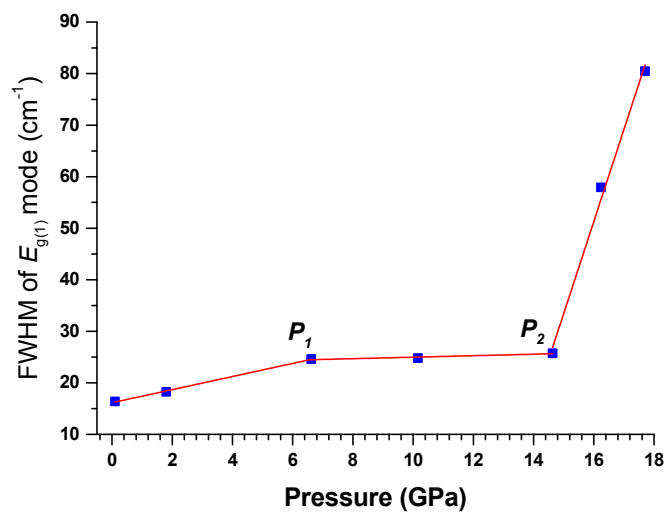
Fig. 5. FWHM of the $E_{g(1)}$ Raman mode as a function of pressure for TiO_2 nanotubes. The solid lines are for eye guidance only. P_1 and P_2 denote the first and second turning pressure points upon compression.
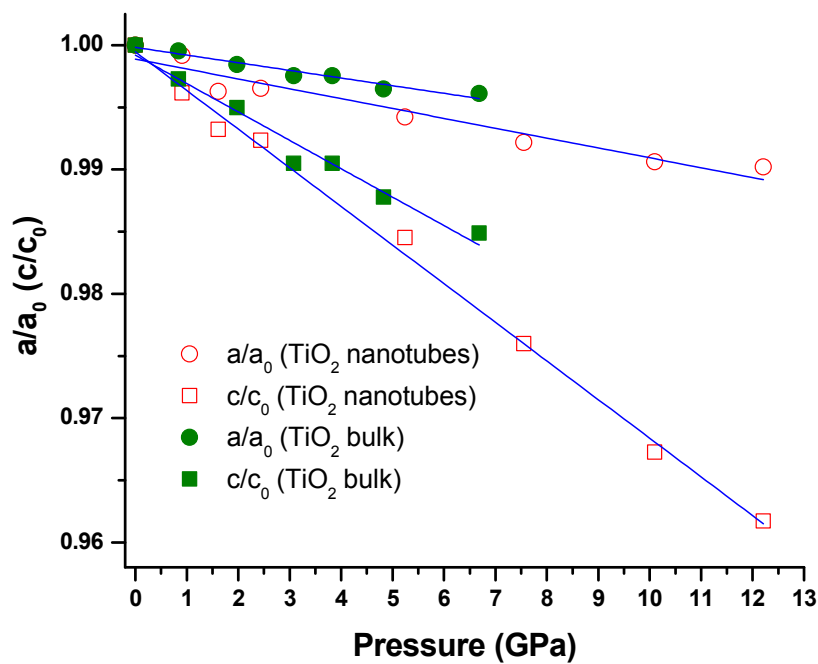
Fig. 6. Pressure dependences of cell parameters of anatase TiO_2 nanotubes in comparison with those of bulk TiO_2. Open and solid symbols denote the cell parameters of the TiO_2 nanotubes and bulk TiO_2 cited from Ref. 24, respectively. Circles and squares represent a/a_0 and c/c_0 ratios, respectively. The solid lines are just for eye guidance.
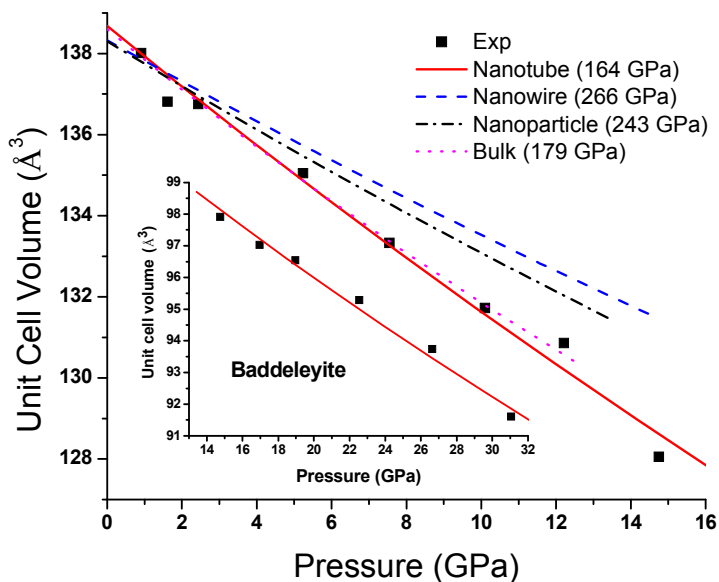
Fig. 7. Pressure dependence of the unit cell volume for the anatase phase of TiO_2 nanotubes in comparison with those for bulk, nanowires, and nanocrystals. The insert figure shows the EOS of baddeleyite phase of TiO_2 nanotubes. Solid squares are from this work. The solid lines represent fitting referring to the third order Birch-Murnaghan equation of state. Dotted lines, dashed lines, and dash dotted lines are the EOS for bulk, nanowires and nanocrystals reported from Ref. 24, Ref. 40 and Ref. 43, respectively.
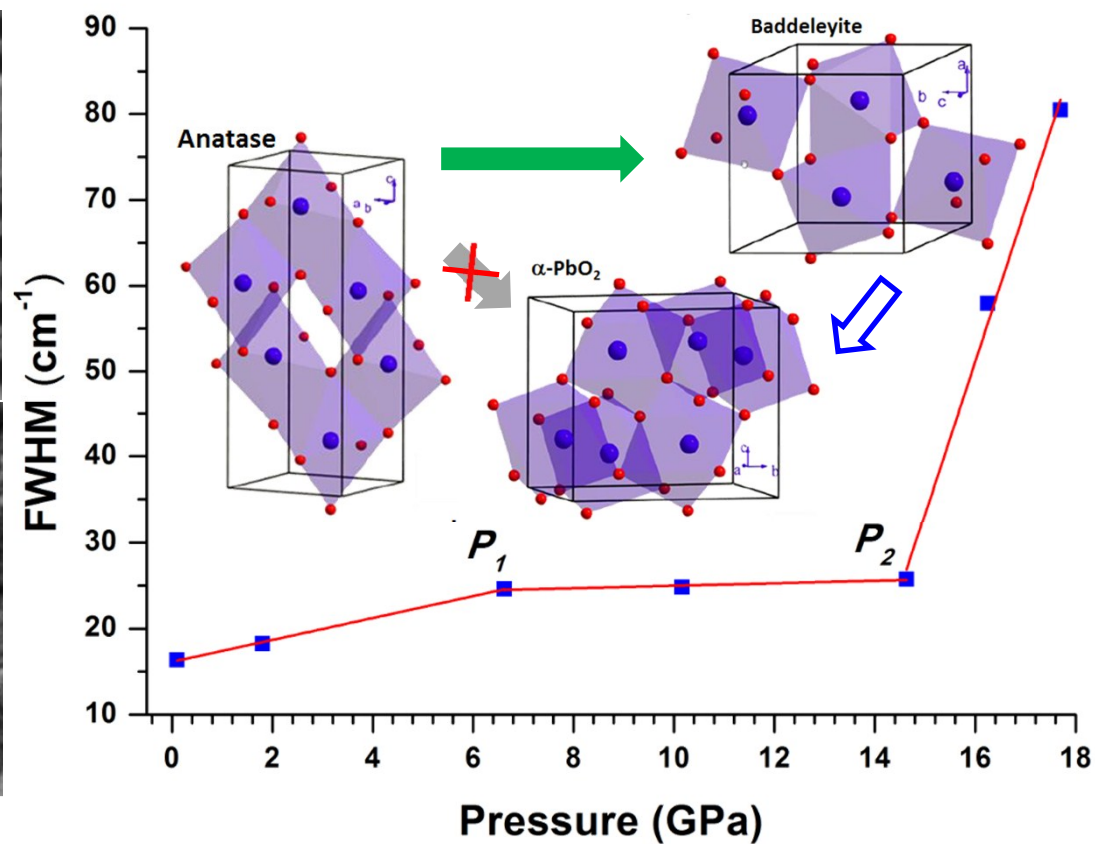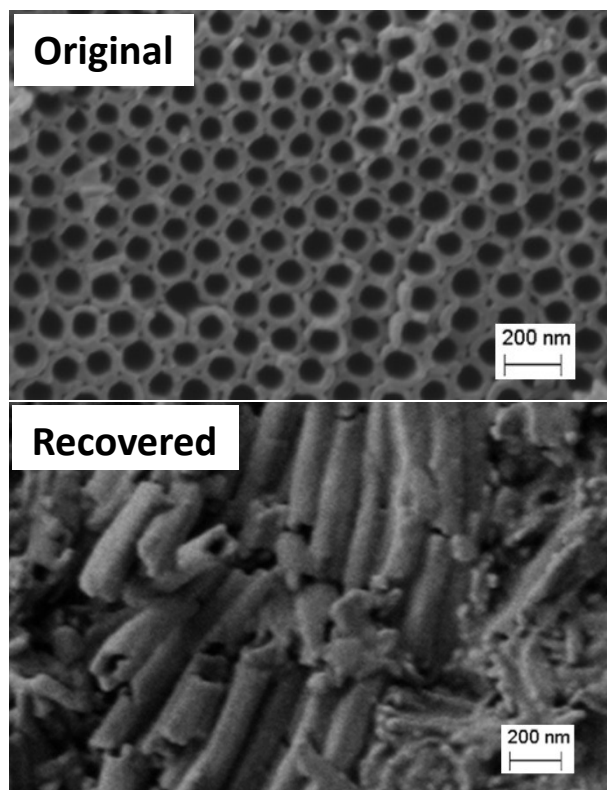
Pressure-induced transformations of anatase TiO_2 nanotubes probed by *in situ* Raman spectroscopy and synchrotron X-ray diffraction reveal novel compression behaviors.